

---

# MMDF: Mobile Microscopy Deep Framework

---

Anatasiia Kornilova<sup>1</sup> Mikhail Salnikov<sup>1</sup> Olga Novitskaya<sup>1</sup> Maria Begicheva<sup>1</sup> Egor Sevriugov<sup>1</sup>  
Kirill Shcherbakov<sup>1</sup>

## Abstract

In the last decade, a huge step was done in the field of mobile microscopes development as well as in the field of mobile microscopy application to real-life disease diagnostics and a lot of other important areas (air/water quality pollution, education, agriculture). In current study we applied image processing techniques from Deep Learning (in-focus/out-of-focus classification, image deblurring and denoising, multi-focus image fusion) to the data obtained from the mobile microscope. Overview of significant works for every task is presented, the most suitable approaches were highlighted. Chosen approaches were implemented as well as their performance were compared with classical computer vision techniques. GitHub repo of the project can be found [here](#).

## 1. Introduction

With the development of optical microscopy technologies, the cost of simple microscopes has become low enough for their mass usage. Considerable role in that class plays mobile microscopy – the field where smartphone camera and computational resources can be used with universal optical microscopes for fast diagnostics in different areas: disease diagnosis (malaria, tuberculosis, some types of cancer in developing countries), on-home diagnostics, agriculture analysis, water and ocean quality and pollution analysis, and education (Bogoch et al., 2013; Shah et al., 2016; Kühnemund et al., 2017; Skandarajah et al., 2017; Wu et al., 2017).

In the past 10 years a lot of solutions were proposed in the field of mobile microscopy — special lenses, devices and classical-look optical microscopes with cheaper optics (Breslauer et al., 2009; Smith et al., 2011; Kim et al., 2015; Jung et al., 2017; Pechprasarn et al., 2018; Orth et al., 2018). In 2015, the research (Skandarajah et al., 2014) shows that the resolution of current wide-spread smart-

phones is good enough to differ important specimen parts in from the mobile microscope. The majority of the works was devoted to the mechanical parts of microscopes to increase the total quality of the image, nonetheless there are a lot of digital processing techniques, especially in Deep Learning, that allows to increase the quality of biomedical microscopic images, like filter in-focus/out-of-focus images, focus-stacking, super-resolution and deblurring, stitching, etc.

The main features of mobile microscopes are bright-field mode (no fluorescence modality), lower quality of images in comparison with professional microscopes, artefacts in optical system (dust, water drops, condensate). All that things don't allow to apply existing algorithms and pre-trained models directly to the mobile microscopy data.

In our work we consider the dataset with z-stack video scanning of 150 specimens from mobile microscope developed by third-party company. All specimens are taken from the standard slide sets produced by AmScope and recorded with 4 speed levels of scanning. Some specimen examples in focused state are demonstrated on the Fig. 1.

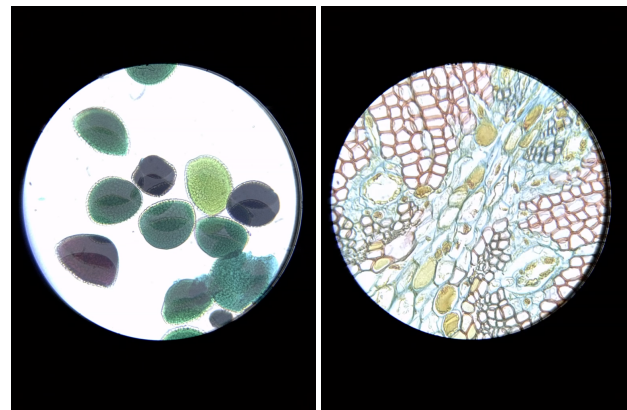


Figure 1. Example of focused images from mobile microscopy dataset

The main techniques that was chosen for our work are following.

- **In-focus/out-of-focus images classification.** Despite auto-focusing systems in modern microscopes, ob-

<sup>1</sup>Skolkovo Institute of Science and Technology, Moscow, Russia. Correspondence to: <anastasiia.kornilova@skoltech.ru>.

tained images are still should be filtered out to remove blurred images with artefacts, to find planes of one specimen with different focused areas. In comparison to classical focus measure operators, Deep Learning techniques allow not to lose small focused parts of the image and ignore artefacts in optical system (dust, drops, condensate).

- **Fast scanning image deblurring.** Obtaining of the high quality images requires much more time while scanning. The idea is to reuse Deep Learning deblurring techniques for fast scanning when we can reconstruct original image from one obtained from the fast movement. Examples of images obtained from fast scanning and slow scanning can be found on the Fig. 2.

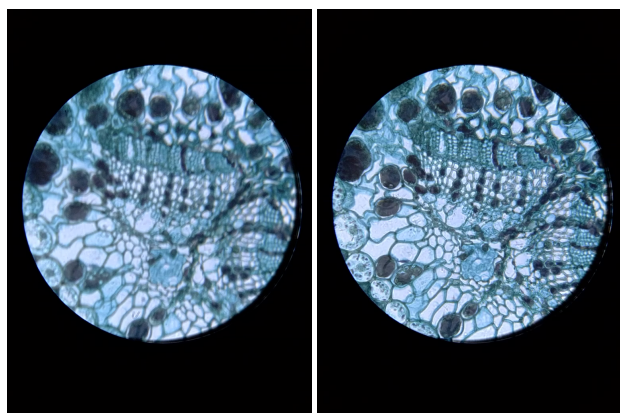


Figure 2. Example of image obtained from fast scan (left) and from slow scan (right)

- **Focus-stacking (Multi-Focus images fusion).** Because of optical microscopes usually have shallow depth of focus, volume specimen can not be studied from one focal length. To understand the specimen structure specialist should study different focal planes of specimen where different areas in focus. The popular technique for that is focus-stacking, or multi-focus image fusion as it is demonstrated on the Fig. 3.

Our main contribution is as follows:

- CNN model for in-focus/out-of-focus classification stable for specific mobile microscopy artefacts was proposed, comparison with other developed solutions in that field was done.
- There was obtained deblurred images with U-Net, SR-CNN and DeblurGAN. The last produced sharper pictures, which is seen in visual comparison with results of baseline models. DeblurGAN results was improved playing with training dataset and removing artefacts with upgrading the standard model.

- FuseGAN model for combining focus parts from several images with a high level of details and smooth transitions for specific mobile microscopy data was proposed, comparison with existed models for this task was done.

## 2. Related work

### 2.1. In-focus/out-of-focus classification

Despite the presence of auto-focusing systems in scanning microscopes, a lot of unfocused images and images with artefacts are produced during specimen recording that increases difficulty of studying sample. The most practical and popular way is to use focus measure operators that took a strong place in all digital imaging. In the paper (Pertuz et al., 2013), authors consider different focus measure operators, classify them into different groups, measure quality and performance. The works (Redondo et al., 2011; Shah et al., 2017) also proposes different focus measure suitable for microscopy and estimate their quality for different types of microscopes.

The main problem of focus measure operators is a lot of false positives in case of dusted images and images with other artefacts. To deal with this the majority of works considers classification task for the whole image using different architectures. The work by (Senaras et al., 2018) considers binary classification task (focused/unfocused) for H&E and IHC-stained slides. Architecture consists of five convolution layers, three max-pooling layers (after the third, fourth and fifth convolution layers) and fully connected layers with categorical cross entropy as objective function. The work by (Kohlberger et al., 2019) presents the same results but focused on the high-resolution slides.

One more important task is not only to detect focused images, but also detect images with different focused areas, therefore more detailed analysis should be done. This part is well-described in the work (Yang S., 2019), where authors consider different parts of the image and estimate focus level for every part using CNN. As the basis authors took all-in-focus images and applied synthetic blurring using PSF based on microscope parameters, assigning different labels for different levels of focus and consider multi-label classification task. The main disadvantage of that method is that it was trained on the data from dark-field fluorescence microscope and can not be applied easily to our case.

### 2.2. Fast image scanning deblurring

Obtaining the high resolution images from blurred images is a classical case in computer vision. In mobile microscopy, algorithmic solutions of this problem allow to use cheaper equipment or fast scanning techniques. The two main direc-

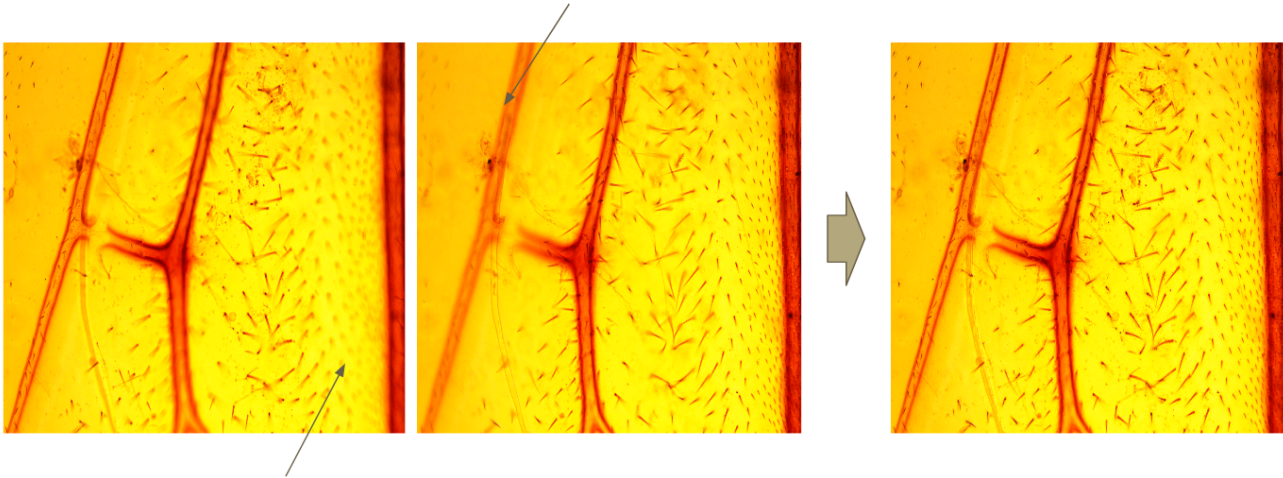


Figure 3. Example of multi-focus images fusion. First two pictures contain partial information about specimen. The right picture demonstrates results of multi-focus images fusion application. Figure by V. Kutuev.

tions of solving deblurring problem are non-blind deblurring and blind deblurring. Early approaches related with the non-blind deblurring such as Lucy-Richardson algorithm or Wiener filtering need to know blur kernel, which finding is not trivial task and depends on the optical system of the device.

The first blind deblurring methods were based on convolutional neural networks (CNN). For instance, Chao Dong et. al proposed simple CNN architecture (Dong C., 2015), which directly learns an end-to-end mapping between blurred and sharp images.

Another type of architecture used for super resolution tasks is autoencoders. Pascal Vincent et. al proposed Denoising Autoencoder (Pascal Vincent, 2008), which directly learns an end-to-end mapping between noisy and clear images in order to extract useful latent representations. In 2010 Pascal Vincent et. al proposed Stacked Denoising Autoencoders (Pascal Vincent, 2010), more complex architecture, which consists of several denoising autoencoders stacked together and trained independently. First autoencoder learns latent representation from picture, then broadcast it to the input of next autoencoder and so on. One more approach is Coupled Deep Autoencoder (CDA) (Kun Zeng, 2017), proposed by Kun Zeng et. al. in 2015. CDA architecture consists of two autoencoders: Source Autoencoder and Target Autoencoder. In one training iteration Source Autoencoder (SA) learns latent representation from noisy image, Target Autoencoder (TA) learns latent representation from clear image, then latent representation from SA is mapped to corresponding TA representation and decoded by TA.

At last time, the generative adversarial networks (GANs)

become popular in solution of different tasks of computer vision including image deblurring (C., 2017). The GANs contain two competitive networks, generator and discriminator. Generator produces deblurring images, discriminator tries to distinguish real images from training dataset and fake images from generator. Besides using the generator and discriminator losses, the perceptual loss of additional pretrained network is included for comparison of deblurred and sharp images. In 2018 Orest Kupyn et. al proposed DeblurGAN (Kupyn O., 2018) allowing to obtain sharp images with motion blurring, which we inspired by.

### 2.3. Image fusion

In general, the image fusion algorithms could be divided in two categories: spatial-domain algorithms and transform-domain algorithms (Xiangzhi Bai, 2015). The spatial-domain image fusion algorithms firstly parse the input images into small blocks or regions according to some criterion, then measure the saliency of the corresponding regions, and finally combine the most salient regions to form the fusion image. Some sophisticated methods, such as guided filtering-based method (GFF) (Li S., 2013), dense SIFT-based method (DSIFT) (Y. Liu, 2015.) have been proposed. The main disadvantages of these algorithms is that they are suitable for fusing images of the same modality. Contrary, the transform-domain image fusion algorithms firstly transform the source images into some feature domain through multi-scale geometric decomposition, and then perform weighted fusion on the features of multiple input images, after which the fused features are inversely transformed to produce the fusion image. Some representative methods contain pyramid decomposition (Liu Z., 2001.),

discrete wavelet transform (DWT) (Tian J., 2012.), etc. This kind of algorithms could be generally used to fuse images with different modalities. However, the fusion strategy or weight coefficients of the transform-domain algorithms are often hard to optimize for the fusion purpose, and thus probably could not achieve the optimal fusion results and suffer from low-contrast effect or blurring effect (Zhang Y., 2020.).

To overcome the problems and limitations of spatial-domain and transform-domain algorithms, Liu et al., recently, presented a convolutional neural networks-based method (CNN) (Liu Y., 2020.), where multi-focus image fusion task was formulated as a classification task and used CNN to predict the focus map. In (H. Tang, 2017.), Tang et al. proposed a CNN model to learn the effective focus-measure and then compared the focus-measures of local image patch pairs of input images to determine the focus map. Afterwards, the above two algorithms both post-processed the focus maps and reconstructed the fusion images according to the refined focus maps. In (K.R. Prabhakar, 2017.), Prabhakar et al. proposed an end-to-end multi-exposure fusion model. More recently, (Zhang Y., 2020.) presented a CNN-based method that utilizes two convolutional layers to extract the salient image features from multiple input images. Afterwards, the convolutional features of multiple input images are fused by an appropriate fusion rule (elementwise-max, elementwise-min or elementwise-mean), which is selected according to the type of input images. Finally, the fused features are reconstructed by two convolutional layers to produce the informative fusion image. However, they all could yield some blurred effects due to the lack of accurate focused regions detection.

More recently, the generative adversarial network introduced by (Ian Goodfellow, 2014.) has achieved great successes in various computer vision tasks. In (Xiaopeng Guo, 2019.) the FuseGAN with dual input-to-one output is proposed to perform the images-to-image task in multi-focus image fusion. However, it may fail to meet situations where the images exist severe misregistration in the dynamic scene. Similarly, in (Xiebo Genga, 2020.) a model based on conditional GAN was introduced that can generate fused images with clear textures and large depth of field without requiring multiple images of different focus depths. However, model results may be poor resolution and the quality of the fused images that are generated by this model on other data styles may decline.

### 3. Algorithms and models

#### 3.1. In-focus/out-of-focus classification

As the basis we took a work (Yang S., 2019) which fits well for characteristics of our task with data from mobile microscopy — it takes into account not the total image quality,

but quality of different parts of image. Authors consider task as multi-label classification where different labels mean different levels of defocus. To obtain different levels of defocus authors used mathematical model of PSF, based on Bessel function, to synthetically defocus all-in-focus images, then random crops of smaller size were generated from the images to create dataset. Since our dataset contains original z-stack of microscope, we used original images from stack with constant step over z-axis instead of synthetic data.

Network architecture is presented on the Fig. 4. It consists of two sequential layers with convolution (kernel size 5x5, stride 1), ReLU activation, maxpooling (2x2 kernel, stride 1). After that, fully connected layer is applied with dropout and softmax. One more important feature of proposed model is to use rank probability score for multi-label classification instead of cross-entropy that shows better results for our task.

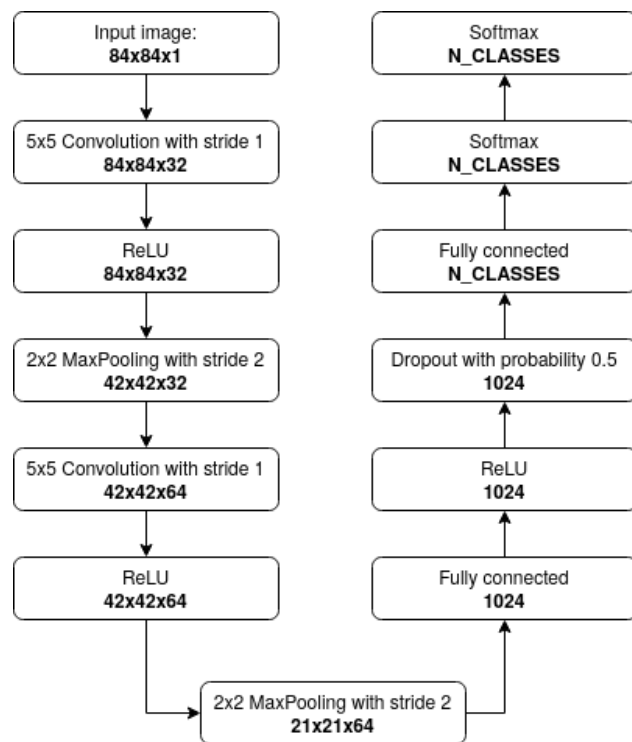


Figure 4. CNN architecture for in-focus/out-of-focus classification

The best parameters for our data were found during experiments and are as follows. Crop size for images —  $84 \times 84$ , number of focus level classes — 10, optimizer — Adam with learning rate  $5 \cdot 10^{-6}$ .

#### 3.2. Fast image scanning deblurring

For obtaining images with high resolution, we decided to check U-net (Ronneberger O., 2015), SRCNN (Dong C.,

2015), DeblurGAN (Kupyn O., 2018), Denoising (Pascal Vincent, 2008), Stacked Denoising (Pascal Vincent, 2010) and Deep Coupled Autoencoders (Kun Zeng, 2017). U-net is familiar in biomedical segmentation, however there are some modifications of this architecture which used in super resolution problems. We decided to use simple U-net with initialization of layers from pretrained VGG11 net (Simonyan K., 2015), it is our baseline model. In addition to this, because of simplicity we used SRCNN. It contains three Conv2d layers 3-64-32-3 and two ReLU activation functions between them. Adam optimizer was used for both nets with learning rate  $10^{-3}$ , training of both nets was provided during 450 epochs.

The main net which showed good performance is DeblurGAN.

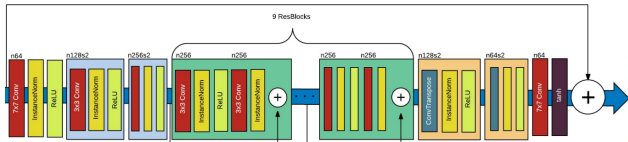


Figure 5. The generator of DeblurGAN model

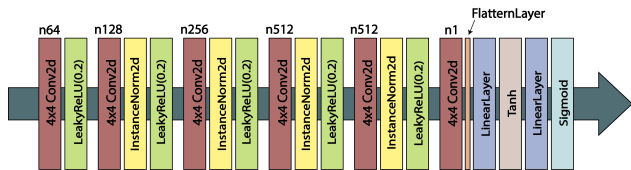


Figure 6. The discriminator of DeblurGAN model

The generator net of DeblurGAN consists of two stride convolution blocks with stride 2, nine residual blocks which keeps track of changes applied to low resolution images, and two transposed convolution blocks. Residual block contains a convolution layer, instance normalization layer, and ReLU activation function.

The discriminator contains sequence of convolution layers, instance normalization, LeakyReLU activation with  $\alpha = 0.2$  and dense layers at the end.

There was used Wasserstein GAN technique with gradient penalty for training. Moreover, the perceptual mean squared error (MSE) loss from VGG19 net (Simonyan K., 2015) was added to generator loss with coefficient 100. This supported net decisions which are perceptually hard to distinguish from high resolution images from the real dataset. Adam optimizers were used for generator and discriminator training with learning rate  $10^{-4}$  and  $\beta_1, \beta_2 = (0.5, 0.999)$ , training of net was provided during 200 epochs.

The standard DeblurGAN model was changed a little bit, because the generator had produced images with color checkerboard pattern of artefacts (Odena A., 2016). The ConvTranspose2d generator layers were replaced with resize-convolution layers. The generator was pretrained minimizing MSE and the structural similarity index measure (SSIM) between generated image and initial input image during 300 epochs. Then training with discriminator occurred with additional term of SSIM between generated and target images in generator loss function. The training was provided during 200 epoch too.

For Denoising Autoencoder we chose encoder with the following structure: five Conv2D layers 3-32-64-128-256-256 with kernel of size 3 and ReLU activation functions between them. BatchNorm2d was applied after every Conv2d layer. For decoder we used symmetric structure with ConvTranspose2d layers. We used Adam optimizer with learning rate  $10^{-4}$ . Number of training epochs is 100. For Stacked Denoising Autoencoder we chose architecture of 3 autoencoders, each of them consists of encoder and decoder. Encoder consists of one Conv2D layer with ReLU activation function after it and decoder consists of one symmetrical ConvTranspose2d layer with ReLU activation function after it. For every autoencoder in layer we chose SGD optimizer with learning rate  $10^{-2}$  and for whole network we chose Adam optimizer with learning rate  $10^{-4}$ . Number of training epochs is 30. For Deep Coupled Autoencoder we chose Source Autoencoder identical to Target Autoencoder. The Target Autoencoder has the structure of Denoising Autoencoder described above. We used Adam optimizer with learning rate  $10^{-7}$  and regularization parameter  $\lambda = 1$ . Number of training epochs is 200.

### 3.3. Image fusion

Our module architecture (Figure 7) consists of three parts: the generator  $G_\theta$ , the discriminator  $D_\theta$ , and the semantic segmentation algorithm for identifying focus regions in input images.

The model from (Xiebo Genga, 2020.) was used as a basis. The generator  $G_\theta$  is an improved version of U-Net model which has an encoder-decoder type of network structure. The plain convolution layers were modified into a DenseBlock modules, which enhance the transfer of the features and makes more efficient use of features compared to common convolutional layers. The input of  $G_\theta$  is a multi-channel image with a width of 720 and a height of 720. Firstly, it will pass through a convolution layer with PReLU outputting a 64-channel feature map. Then, there will be three DenseBlocks and three average pooling layers. The DenseBlocks in the encoding stage (the left branch in Figure 8) consists of a common convolution layer and two DenseBlock blocks. The DenseBlock in our network only use

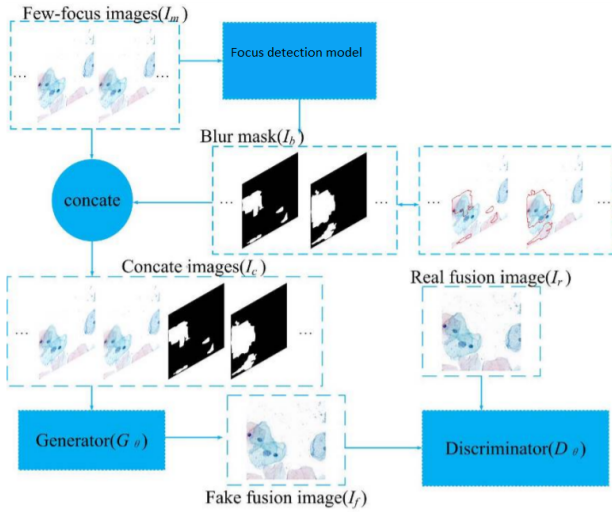


Figure 7. Supervised FuseGAN model architecture

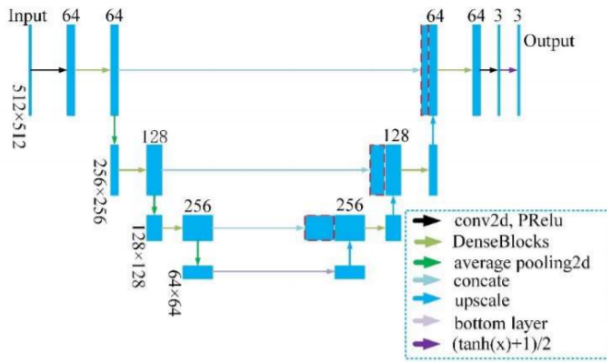


Figure 8. The generator of FuseGAN model

a 3-layer convolution, thereby reducing the computational overhead. When reaching the bottom of U-Net, it will go through the bottom layer, which is a 3-layer convolution with PRelu. During the decoding stage, the network goes through three bilinear upsampling layers, and each layer is followed by a DenseBlocks. Different from the encoding stage, the input of the DenseBlocks in decoding stage is concatenated by the output of the bilinear upsampling layer and the corresponding DenseBlocks output of the encoding stage. At the top of the network, the convolutional layer and the active tanh layer are used to reduce the number of channels of the feature map and normalize it to between 0 and 1, thereby obtaining a 3-channel output.

The PatchGAN discriminator  $D_\theta$  here uses a structure similar to the VGG.  $D_\theta$  consists of 8 convolution layers with LeakyReLU, a maximum pooling layer with a window size of 4 and a stride size of 4, and a sigmoid activation layer.  $D_\theta$

outputs an  $N \times N$  map with values between 0 and 1. The receptive field of each point of the output map corresponds to a small patch of the input image. The size of the patch here is  $64 \times 64$ , which makes the discriminator pay more attention to the local details.

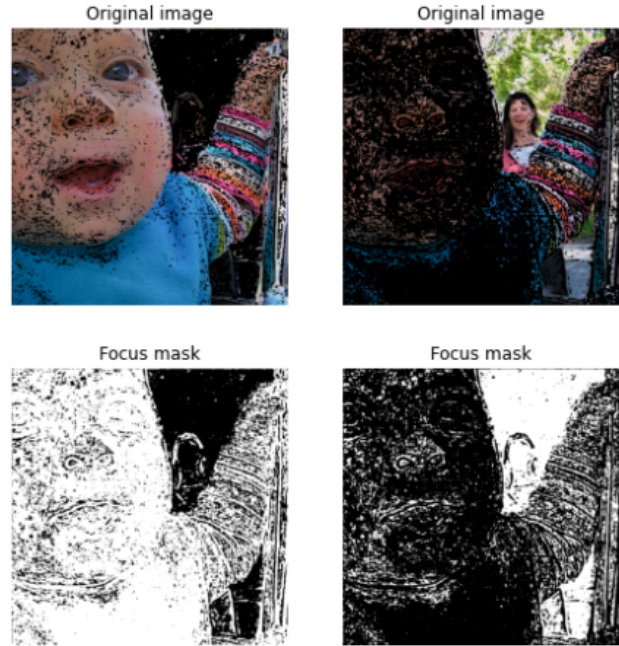


Figure 9. Modified Harris Corner Response Measure algorithm example

To make masks (Figure 9) for general model Modified Harris Corner Response Measure (Madhu et al., 2015) was used. It is based on calculation of the derivatives over the image intensity to define regions which were blurred and which not. Model as input gets images which already multiplied on this mask in order to not provide information on blurred regions.

In training process for discriminator the following loss was used:

$$\text{BCELoss}(\text{fake}, 0) + \text{BCELoss}(\text{real}, 1),$$

where fake - images generated by generator model, real - ground truth.

For generator loss several options are tested:

1. BCELoss + L1Loss
2. BCELoss + L1Loss + Perceptual loss(using VGG16(Justin et al., 2016)), sFUSE
3. BCELoss + L1Loss + Perceptual loss(using discriminator) sFuseGAN

4. BCELoss + uL1Loss + Perceptual loss(using discriminator) *uFuseGAN*

Here L1Loss - mean absolute error calculated between model output and ground truth, Perceptual loss - loss calculated on hidden outputs of VGG16/discriminator, uL1Loss - updated mean absolute error calculated between model output multiplied by corresponding mask and input images multiplied by corresponding mask.

## 4. Experiments and results

### 4.1. In-focus/out-of-focus classification

#### 4.1.1. DATASET

For our experiment we created dataset that contains 45 specimens with all-in-focus images. 20 levels of blur were provided for every specimen using z-stack frames from the video scanning. For training, fixed size random crops of full images was chosen. For test, we chose 100 focused and 100 unfocused crops, hand-labeled in binary manner — 1 means unfocused crop, 0 means focused crop. Also, using binary threshold from OpenCV, mask for specimen was created to escape of random crops in black area of image (Fig. 10). As library for augmentations Albumentations was used. Since dataset was not large, it was read in RAM entirely.

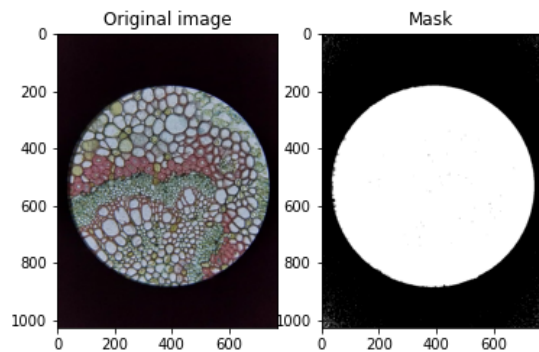


Figure 10. Mask detection which is used to avoid crops without specimen parts

#### 4.1.2. EVALUATION

For evaluation we considered binary classification task and accuracy metric, since our test dataset is well-balanced.

#### 4.1.3. INTERESTINGNESS OF RESULTS

In our comparison we consider the most significant operators from microscopy focus measure operators reviews (Re-dondo et al., 2011; Shah et al., 2017) (Laplacian, Tenengrad, Vollath), original pre-trained model from the paper (Yang S.,

2019) and our upgraded model. We also took into comparison a popular pre-trained model for non-microscopic images from the paper by (Hsu & Chen, 2008), based on SVM model.

Table 1. Accuracy comparison for focused classification task (CI = 95%).

APPROACH	ACCURACY
FOCUS MEASURES	55%
SVM	40%
ORIGINAL MODEL	$79 \pm 2 \%$
OURS	<b><math>95,6 \pm 2,8 \%</math></b>

Experiments show that proposed approach in our work has better performance. Without fear of favor, the main reason is that all considered approaches are suited well for their specific task and works bad on other type of the data. The main contribution of that part is sustainability of approach for false positives on the dusted images and images with artefacts.

Application of that algorithm is demonstrated on the Fig. 11. The input image is cut into grid of smaller images, every image is evaluated over trained network. According to the predicted class, the crop is marked into different colors, where green means high level of blur, red means low level of blur.

One of the arose problem was false positives on crops with dust and water drops that should be marked as not-focused (Fig. 12), but in the original state model showed bad performance on those cases. To deal with that problem, we extended our dataset with dusted images with label equal to unfocused images.

### 4.2. Fast image scanning deblurring

#### 4.2.1. DATASET

Our mobile microscopy dataset contains videos from fast and slow scanning. We decided to chose 192 pairs of blurred and sharp images from slow scanning for training. The initial image size is  $768 \times 1024$ . So, for faster computations we cropped images to a square containing a circle with a sample and resized to  $256 \times 256$ .

In the following experiment we decided to replace all naturally blurred input images with our own low resolution images with blur kernel (size=4, variance= $1.25 \cdot 10^{-2}$ ) inspired by idea of DeblurGAN article.

In addition to this, we used a combination of wild blurred and synthetically blurred images: the common quantity of wild blurred images was 192, 119 images with small blur kernel (size=4, variance= $1.25 \cdot 10^{-2}$ ) and 119 images with large blur (size=15, variance= $1.67 \cdot 10^{-2}$ ) were added to

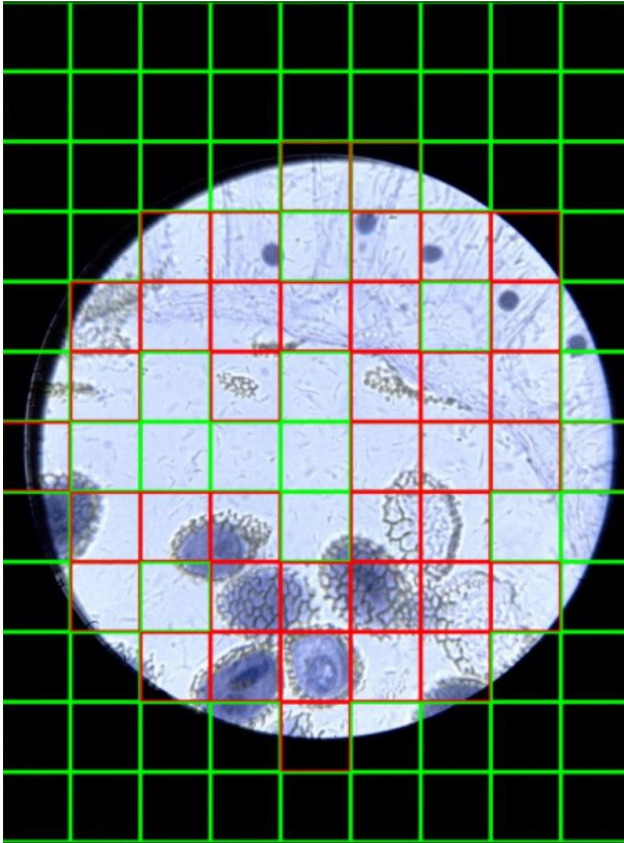


Figure 11. Example of proposed network for in-focus/out-of-focus application

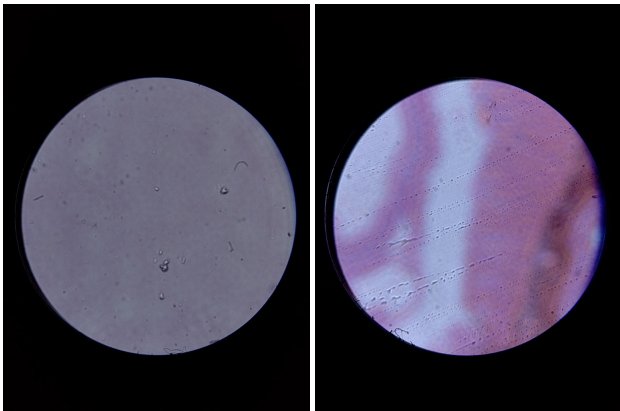


Figure 12. Example of images with artefacts that can be classified as focused

them.

For testing, we used blurred images resized to  $256 \times 256$  from fast scanning.

Also, during pretraining generator we cropped  $256 \times 256$  images to  $64 \times 64$  size and used transformations such as random horizontal flip, random vertical flip and random ro-

Table 2. Comparison of results obtained with 3 nets (mean over 8 test samples, CI = 95%).

	PSNR	SSIM, $10^{-2}$
BLURRED IMAGE	$29.20 \pm 9.27$	$86.88 \pm 14.32$
U-NET	$26.72 \pm 4.77$	$81.96 \pm 9.60$
SRNET	$28.80 \pm 7.83$	$86.33 \pm 11.73$
UDEBLURGAN	$28.33 \pm 8.09$	$84.58 \pm 13.76$
SDEBLURGAN	$24.49 \pm 5.23$	$62.54 \pm 18.26$

Table 3. Comparison of DeblurGAN results, trained on different sets (mean over 8 test samples, CI = 95%).

	PSNR	SSIM, $10^{-2}$
BLURRED IMAGE	$29.20 \pm 9.27$	$86.88 \pm 14.32$
SDEBLURGAN, WILD BLUR	$24.49 \pm 5.23$	$62.54 \pm 18.26$
SDEBLURGAN, SYNTHETIC BLUR	$23.85 \pm 4.04$	$68.75 \pm 11.39$
SDEBLURGAN, MIX BLUR	$24.61 \pm 4.39$	$69.40 \pm 9.12$

tation for data augmentation. After pretraining of upgraded generator, training of whole DeblurGAN was provided on the wild blurred images with size  $256 \times 256$ .

#### 4.2.2. EVALUATION

For evaluation the quality of deblurred images we used peak signal-to-noise ratio (PSNR) and SSIM metrics, also we compared generated images with input and target visually.

#### 4.2.3. INTERESTINGNESS OF RESULTS

The results of U-Net, SRCNN, upgraded and standard DeblurGAN (DGAN) deblurring are presented on Figure 13. B) C) D) E): Models were trained on the wild blurred images, which were used as an input for the generator. U-net and SRCNN images look like blurred, DeblurGAN gives pictures with clearer lines. F) G): the results of standard DeblurGAN trained on several variations of datasets are presented; F): trained on all synthetically blurred images; G): trained on the large dataset, contained a combination of 192 wild blurred and synthetically blurred images, 238 additional images with small blur kernel and with large blur kernel.

In tables 2 and 3 the comparison of results with PSNR and SSIM metrics. sDeblurGAN results don't look very good in comparison with blur images, which have high values of metrics. We guessed that the cause is the existence of color checkerboard pattern of artefacts obtained with deconvolution of blurred image.

We have improved the base DeblurGAN model with resize-convolution layers and pretraining, in such a way we have avoided artefacts. Both metrics describing the quality of



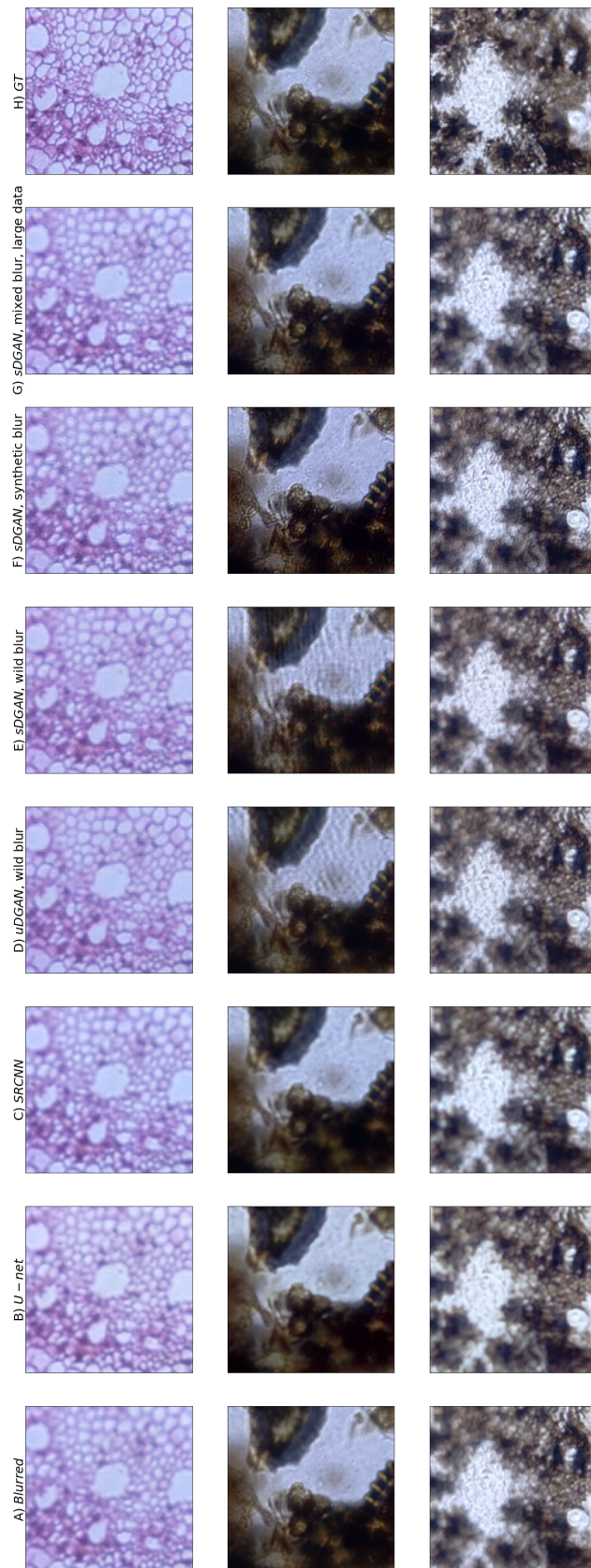


Figure 13. A): crop of blurred image. B), C), D), E): comparison of U-net, SRCNN, uDGAN and sDGAN on wild blurred images. F), G): results of sDGAN trained on synthetically blurred images and on the mixture of wild and synthetic blurred data. H): ground truth. The subscripts s and u denote standard and upgraded, respectively

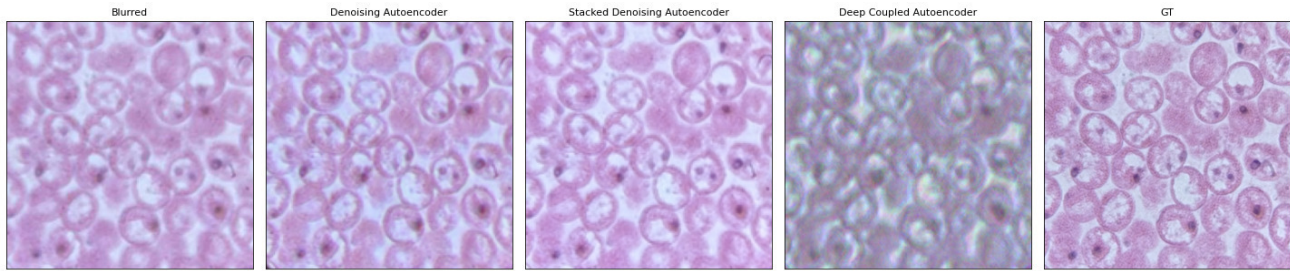


Figure 14. Comparison of Denoising, Stacked Denoising and Deep Coupled Autoencoders work on wild blurred training dataset

images generated with uDeblurGAN are better than metrics applied to sDeblurGAN pictures. U-net, SRNet results and blurred images have highest values of PSNR and SSIM but pictures haven't good quality in visual comparison. So, for the rude quality evaluation these metrics work. On the other hand, they fail in more accurately assess of image quality(C., 2017).

According to the visual comparison the sDeblurGAN trained on large mixed dataset gives sharper results than initial blurred image. Its PSNR and SSIM metrics are best among standard DeblurGAN trained on different types of data. In further plans, we will combine uDeblurGAN model and large mixed dataset for reaching better accuracy of deblurring

Experiments with autoencoders mentioned in report didnt show satisfying results. On Figure 14 there are presented results of Denoising, Stacked Denoising and Deep Coupled Autoencoder deblurring. These models were trained on the wild blurred images. First picture is blurred image, second - the result of Denoising Autoencoder, third - the result of Stacked Denoising Autoencoder, fourth - Deep Coupled Autoencoder, the last picture - ground truth image (GT). Denoising Autoencoder and Stacked Denoising Autoencoder didnt show improvement of initial blurred image. Deep Coupled Autoencoder changed colour channels of pictures and didn't remove blur. We suggest, autoencoders are too simple architectures for such kind of tasks.

Creating additional google accounts for experiments equals 4, summary count of google accounts for solving deblurring problem are 8.

### 4.3. Image fusion

#### 4.3.1. DATASET

Images of all specimens obtained in a super slow mode (94 specimens) as well as multi-focus images fusion results obtained by using wavelet transform and by using pre-trained CNN (IFCNN, the state-of-the-art model for fusion task) with two fusion rule strategies (elementwise-max and

elementwise-mean) were selected and preprocessed, and duplicate images were removed. Specifically, we resized all specimens to  $720 \times 720$ . Additionally, we added the Lytro Multi-Focus fusion dataset (20 samples) that was created similarly to naturally captured images that have focused and blurred areas due to the characteristics of optical lens. We divided the data into 95% training and 5% testing. We also use data augmentation during training due to the small size of the dataset. Especially we use horizontal flip, rotate, vertical flip and shift-scale-rotate with probability of each transformation 0.5.

#### 4.3.2. TRAINING

We trained FuseGAN model without and with masks obtained by Harris Corner Response Measure algorithm with all the options of the generator loss mentioned above.

Specifically, in training procedure all input images for particular sample with different focus regions are merged over second dimension(channels). When we add mask we simply merged input images with masks in second dimension. In order to have equal sized tensors as model input we add to samples, with less number of images, additional channels with zeros.

To calculate perception loss we have tried two options as it were mentioned above: one gotten from use of VGG16(Justin et al., 2016) and other from use of discriminator. In particular, VGG16 model is already made in the way to provide hidden representation, in other words outputs of several blocks inside model. And to calculate loss we passed ground truth and generator output throw this model, and calculate the difference between obtained hidden representations. In the same manner we work with discriminator, simply split its structure on several blocks and return not only the final output but the middle too.

Moreover to achieve more detailed pictures we have tried semi-supervised learning (Fig. 15). Originally to train generator we add to BCELoss additional term: L1Loss, which is measured the difference between output of the

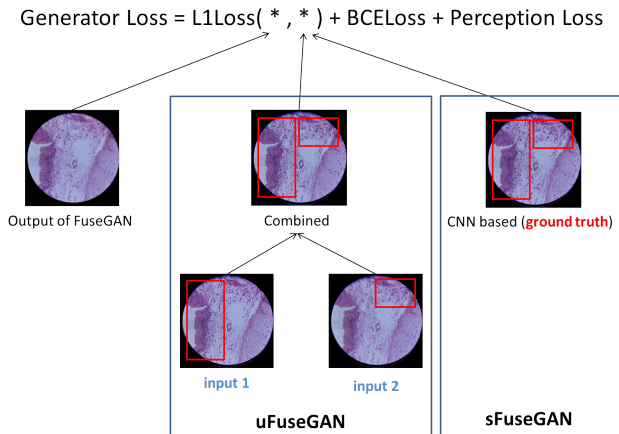


Figure 15. Implementation of semi-supervised learning

Table 4. Performance of fusion models (mean over test samples). The subscript *s* and *u* denote standard and upgraded, respectively (CI = 95%).

MODEL	BRISQUE	CNNIQA
<b>uFUSEGAN</b>	$37.21 \pm 3.48$	$25.71 \pm 4.36$
<b>sFUSEGAN</b>	$40.59 \pm 4.66$	$32.44 \pm 5.44$
WAVELET TRANSFORM	$31.83 \pm 3.12$	$23.47 \pm 3.01$
<b>IFCNN</b>	$36.19 \pm 3.23$	$25.97 \pm 4.48$

model and ground truth, but this is useful only in the case, when we really have good target image. In our case the target image is not quite well, and because of this we replace this loss by new one which measure the difference between focus parts on each input image and corresponding part in output.

#### 1. Discriminator optimal parameters

- Optimizer Adam:  $lr = 4 \cdot 10^{-5}$ ,  $betas = (0.0, 0.999)$
- Scheduler StepLR:  $stepsize = 1$ ,  $gamma = 0.95$
- Loss:  $1 * BCELoss(fake, 0) + 1 * BCELoss(real, 1)$

#### 2. Generator optimal parameters

- Optimizer Adam:  $lr = 5 \cdot 10^{-5}$ ,  $betas = (0.0, 0.999)$
- Scheduler StepLR:  $stepsize = 1$ ,  $gamma = 0.95$
- Loss:  $2 * L1Loss + 0.001 * BCELoss + 1 * PerceptionLoss$

#### 4.3.3. EVALUATION

During evaluating the image fusion algorithms, we have adopted both qualitative and quantitative methods to discriminate the performance of different image fusion algorithms. Firstly, qualitative evaluation is performed by judging the visual effects of their fusion images with respect to the source images. To be specific, whether the visual effects of fusion images are satisfying for each type of image dataset can be judged by the following criteria: multi-focus image fusion should integrate as much clear and sharp features as possible from each source image into the fusion image. Besides the above criteria, another important criterion is that the fusion images should look as natural as possible so that the human eyes can easily and accurately obtain the comprehensive information from the fusion image. Since there is no ground-truth image for MMDF task, the no-reference quantitative image assessment metrics are widely employed in this case. A pretrained CNN (CNNIQA) (Kang et al., 2015) that generates image quality predictions well correlated with human perception and can estimate quality in local regions and a natural scene statistic based distortion generic blind/no-reference (NR) quality assessment algorithm - the Blind/Referenceless Image Spatial Quality Evaluator (BRISQUE) (Mittal A, 2012.) that is statistically better than FR PSNR and SSIM as well as highly competitive to all NR algorithms compared with were used for no-reference quantitative image quality assessment.

An anonymous survey to determine the best algorithm for ground truth images for FuseGAN training, which included randomly mixed images from wavelet transform algorithm and IFCNN, showed that qualitatively the best model is IFCNN elementwise-max model by the dominant decision of 28 respondents. Quantitatively we obtained that the best ground truth images from wavelet transform algorithm and IFCNN elementwise-max model with BRISQUE mean score 31.83 and 36.19 and CNNIQA mean score 23.47 and 25.97 respectively. All qualitative results are presented in Figure 16 and all quantitative results are presented in Table 4. The highest FuseGAN CNNIQA and BRISQUE mean scores over all test specimens was at unsupervised FuseGAN with 25.71 and 37.21 as well as the best qualitative performance.

#### 4.3.4. INTERESTINGNESS OF RESULTS

Firstly, we started training with the generator loss that does not contain perceptual loss part, having MAE loss (between a generated image and the target) and BCE loss parts. Searching for the best loss coefficients and evaluating with our findings, we saw that the model perform well with color restoration and the structure of the source image but it could not manage to obtain decent resolution (see Figure 17) and tend to make it blurry.

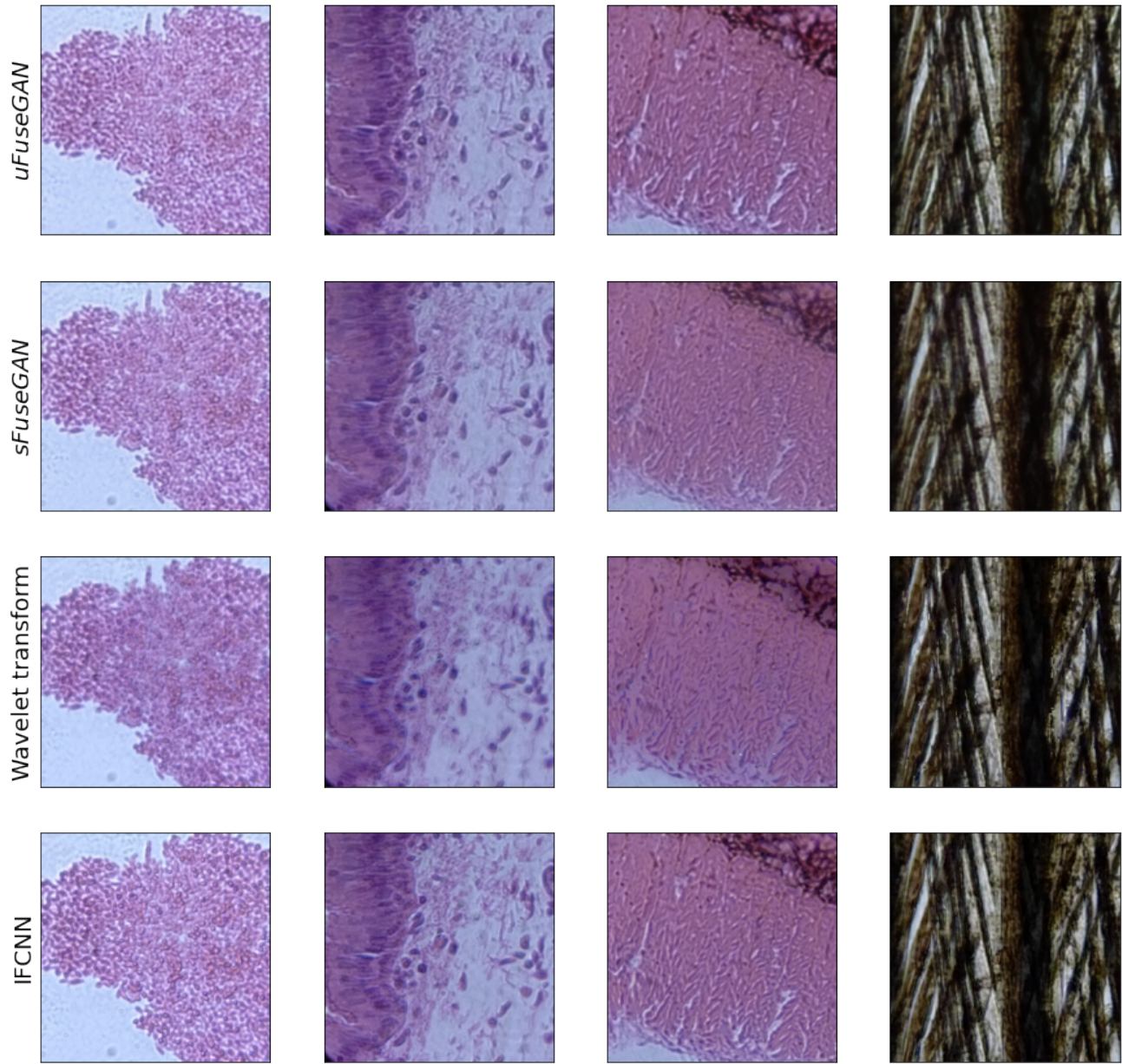


Figure 16. Comparison of considered fusion algorithms

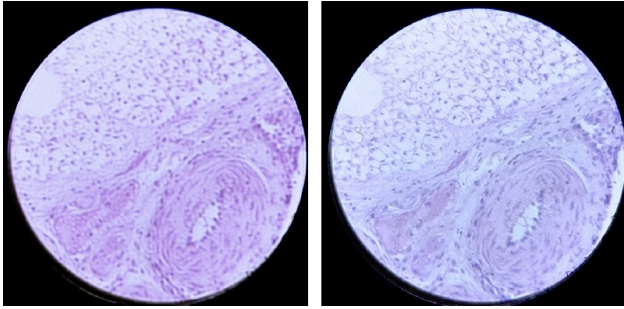


Figure 17. Example of FuseGAN generator output training with loss without perceptual loss part (right picture - output of the generator, left picture - target image)

Moreover, we found that for the perceptual loss for our specific data features from pretrained VGG16 shows worse performance than the features from convolutions layers of our discriminator. The distinctive difference was that the perceptual loss with VGG16 output features slightly changed colors of output images compared with colors of target images.

Another interesting result is that qualitatively (visually judging output from the IFCNN images and output from wavelet transform algorithm images, Figure 16) output images from the IFCNN is much better and look more natural for a human eye than output images from wavelet transform algorithm, and the anonymous survive with 28 respondents proved that. However, all quantitative metrics (Figure 4) show vice versa. The reason could be that wavelets transform is a transform-based algorithm, i.e. they translate images to another domain, glue them together there, and reverse the transformation. Therefore, the image turns out to be smooth, with smooth transitions. Contrary, the proposed methods have pixel-based approach, so it can still get non-smooth transitions that are invisible to human eye, and the metrics show that.

To generate mask firstly we have tried approach proposed in article. But the masks obtained in this way were completely useless. Since this method did not produce the expected results, the other two methods were taken into consideration (Figure 18). One of them is based on the model described in the In-focus/out-of-focus classification(BM on figure - blurring model) part of the current report, the other is based on the Modified Harris Corner Response Measure (Figure 18). As you can easily see in the comparison picture, BM works well in detecting blurring regions, but it is insensitive to details, which is a very important property in the case of biomedical images. As a result, a model based on the Modified Harris Corner Response Measure algorithm was selected for the project because it demonstrated high sensitivity to details.

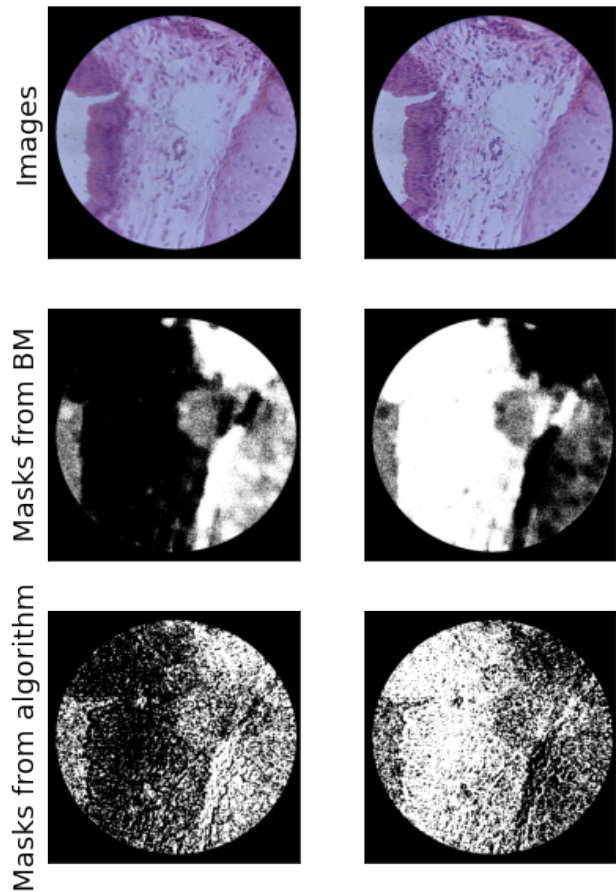


Figure 18. Comparison of different approaches for mask generation

## 5. Conclusion

In our work we considered different networks proposed in the microscopy field for image quality assessment, found out the requirements for our task and chose the most suitable one. The approach was improved and adopted for our data. Several hypothesis with false positives on dust were tested, accuracy more than 95% on test images was achieved.

Also, there were tested various models for obtaining sharp denoised images: U-Net, SRCNN, DeblurGAN, Denoising Autoencoder, Stacked Denoising Autoencoder, Deep Coupled Autoencoder. According to the results, DeblurGAN generates sharper images than other methods. Adding the synthetically blurred images in training dataset and increasing the number of training pictures improves the quality of output testing images. We resolved the problem of the existence of some artefacts in output images, which affects negatively on the computing of metrics. However, standard PSNR and SSIM metrics fail to provide fine comparison of images.

In our work we considered different techniques for improving quality of images obtained from z-stack scanning from mobile microscope. Despite the fact that we managed to achieve qualitative improvements for the image fusion task, we did not manage to improve the quantitative metrics that we chose for evaluating our models. Wavelets transform is a transform-based algorithm, i.e. they translate images to another domain, glue them together there, and reverse the transformation. Therefore, the image turns out to be smooth, with smooth transitions. Contrary, the proposed methods have pixel-based approach, so it can still get non-smooth transitions that are invisible to human eye, and the metrics show that. Therefore, based on visual improvements, we can conclude that we successfully solve the image fusion task with proposed FuseGAN model.

## 6. Further works

### 6.1. Image fusion

Applying of in-focus/out-of-focus algorithms is important on the smartphone side to significantly decrease the network traffic, therefore additional experiments should be conducted to measure performance of the network and, probably, to make it more lightweight.

In this work we tested upgraded DeblurGAN model on the small wild blurred dataset, the next step will be the training of uDeblurGAN on synthetically blurred images and on the large mixed data. Also we think about experimenting with other neural networks, for example EDVR.

In future version the best model parameters will be found for FuseGAN. In particular, there were artefacts on some images produced by our model. One of the possible reason of such mistakes is not appropriate loss coefficients. In addition, more useful hidden features could be chosen for perceptual loss to improve quality of generated images.

## 7. Acknowledgement

We would like to express our gratitude to the company MEL Science that provided mobile microscopy dataset. Also, we would like to pay our regards to Deep Learning (Prof. Lempitsky) and Biomedical Imaging and Analytics (Prof. Dylov) courses lecturers and teaching assistants, especially Valeriya Pronina for our supervising and invaluable advice.

## References

Bogoch, I. I., Andrews, J. R., Speich, B., Utzinger, J., Ame, S. M., Ali, S. M., and Keiser, J. Short report: Mobile phone microscopy for the diagnosis of soil-transmitted helminth infections: A proof-of-concept study. *American Journal of Tropical Medicine and Hygiene*, 88(4):626–

629, 2013. ISSN 00029637. doi: 10.4269/ajtmh.12-0742.

Breslauer, D. N., Maamari, R. N., Switz, N. A., Lam, W. A., and Fletcher, D. A. Mobile phone based clinical microscopy for global health applications. *PLoS ONE*, 4(7): 1–7, 2009. ISSN 19326203. doi: 10.1371/journal.pone.0006320.

C., L. Photo-Realistic Single Image Super-Resolution Using a Generative Adversarial Network. *arXiv:1609.04802v5*, 2017.

Dong C., Loy C., H. K. Image Super-Resolution Using Deep Convolutional Networks. *arXiv:1501.00092v3*, 2015.

H. Tang, B. Xiao, W. L. Pixel convolutional neural network for multi-focus image fusion. *Inf. Fusion.*, 8:821–829, 2017.

Hsu, P. and Chen, B. Y. Blurred image detection and classification. *Lecture Notes in Computer Science (including sub-series Lecture Notes in Artificial Intelligence and Lecture Notes in Bioinformatics)*, 4903 LNCS:277–286, 2008. ISSN 03029743. doi: 10.1007/978-3-540-77409-9\_26.

Ian Goodfellow, Jean Pouget-Abadie, M. M. Generative adversarial nets. *Advances in neural information processing systems*, 8:2672–2680, 2014.

Jung, D., Choi, J. H., Kim, S., Ryu, S., Lee, W., Lee, J. S., and Joo, C. Smartphone-based multi-contrast microscope using color-multiplexed illumination. *Scientific Reports*, 7(1):1–10, 2017. ISSN 20452322. doi: 10.1038/s41598-017-07703-w. URL <http://dx.doi.org/10.1038/s41598-017-07703-w>.

Justin, Johnson, A., Alahi, L., and Fei-Fei. Perceptual losses for real-time style transfer and super-resolution. *arXiv preprint arXiv:1603.08155*, 2016.

Kang, L., Ye, P., Li, Y., and Doermann, D. Simultaneous estimation of image quality and distortion via multi-task convolutional neural networks. pp. 2791–2795, 2015.

Kim, J. H., Joo, H. G., Kim, T. H., and Ju, Y. G. A smartphone-based fluorescence microscope utilizing an external phone camera lens module. *Biochip Journal*, 9(4):285–292, 2015. ISSN 20927843. doi: 10.1007/s13206-015-9403-0.

Kohlberger, T., Liu, Y., Moran, M., Chen, P. H., Brown, T., Hipp, J., Mermel, C., and Stumpe, M. Whole-slide image focus quality: Automatic assessment and impact on ai cancer detection. *Journal of Pathology Informatics*, 10 (1), 2019. ISSN 21533539. doi: 10.4103/jpi.jpi\_11\_19.

K.R. Prabhakar, V.S. Srikar, R. B. Deepfuse: a deep unsupervised approach for exposure fusion with extreme

- exposure image pairs. *IEEE Trans. Image Process.*, 8: 47244732, 2017.
- Kühnemund, M., Wei, Q., Darai, E., Wang, Y., Iván, H. N., Yang, Z., Tseng, D., Ahlford, A., Mathot, L., Sjöblom, T., Ozcan, A., and Nilsson, M. Targeted DNA sequencing and in situ mutation analysis using mobile phone microscopy. *Nature Communications*, 8:1–8, 2017. ISSN 20411723.
- Kun Zeng, Jun Yu, R. W. Coupled deep autoencoder for single image super-resolution. *IEEE Transactions on Cybernetics*, 47:27–37, 2017.
- Kupyn O., Budzan V., M. M. DeblurGAN: Blind Motion Deblurring Using Conditional Adversarial Networks. *arXiv:1711.07064v4*, 2018.
- Li S., Kang X., H. J. Image fusion with guided filtering. *IEEE Trans. Image Process.*, 22:28642875, 2013.
- Liu Y., Chen X., P. H. Multi-focus image fusion with a deep convolutional neural network. *Inf. Fusion.*, 9:191–207, 2020.
- Liu Z., Tsukada K., H. K. Image fusion by using steerable pyramid. *IEEE Trans. Image Process.*, 9:929939, 2001.
- Madhu, Sigdel, M., Sigdel, S., Dinc, I., and Dinc. Focusall: Focal stacking of microscopic images using modified harris corner response measure. *IEEE/ACM Transactions on Computational Biology and Bioinformatics*, 2015.
- Mittal A, Moorthy AK, B. A. No-reference image quality assessment in the spatial domain. *IEEE Trans. Image Process.*, 8:2672–2680, 2012.
- Odena A., Dumoulin V., O. C. Deconvolution and checkerboard artifacts. 2016.
- Orth, A., Wilson, E. R., Thompson, J. G., and Gibson, B. C. A dual-mode mobile phone microscope using the onboard camera flash and ambient light. *Scientific Reports*, 8(1):1–8, 2018. ISSN 20452322. doi: 10.1038/s41598-018-21543-2. URL <http://dx.doi.org/10.1038/s41598-018-21543-2>.
- Pascal Vincent, Hugo Larochelle, I. L. Extracting and composing robust features with denoising autoencoders. In *Proceedings of the 25th international conference on Machine learning (ICML 2008)*, pp. 1096–1103, Association for Computing Machinery, New York, NY, United States, 2008.
- Pascal Vincent, Hugo Larochelle, I. L. Stacked denoising autoencoders: Learning useful representations in a deep network with a local denoising criterion. *Journal of Machine Learning Research*, 11:3371–3408, 2010.
- Pechprasarn, S., Pimonsakonwong, P., Kulikhandan, P., Suvarnaphaet, P., Pongruengkiat, W., Suksan, P., and Albutt, N. Compact Fluorescence Microscope for Smartphone and Tablet. *Applied Mechanics and Materials*, 879:222–226, 2018. doi: 10.4028/www.scientific.net/amm.879.222.
- Pertuz, S., Puig, D., and Garcia, M. A. Analysis of focus measure operators for shape-from-focus. *Pattern Recognition*, 46(5):1415–1432, 2013. ISSN 00313203. doi: 10.1016/j.patcog.2012.11.011.
- Redondo, R., Bueno, M. G., Valdiviezo, J. C., Nava, R., Cristóbal, G., García, M., Déniz, O., and Escalante-Ramírez, B. Evaluation of autofocus measures for microscopy images of biopsy and cytology. *22nd Congress of the International Commission for Optics: Light for the Development of the World*, 8011:801194, 2011. ISSN 0277786X. doi: 10.1117/12.903314.
- Ronneberger O., Fischer P., B. T. U-Net: Convolutional Networks for Biomedical Image Segmentation. *arXiv:1505.04597v1*, 2015.
- Senaras, C., Khalid Khan Niazi, M., Lozanski, G., and Gurcan, M. N. DeepFocus: Detection of out-of-focus regions in whole slide digital images using deep learning. *PLoS ONE*, 13(10):1–13, 2018. ISSN 19326203. doi: 10.1371/journal.pone.0205387.
- Shah, M. I., Mishra, S., Sarkar, M., and Sudarshan, S. K. Automatic detection and classification of tuberculosis bacilli from camera-enabled smartphone microscopic images. In *2016 Fourth International Conference on Parallel, Distributed and Grid Computing (PDGC)*, pp. 287–290, 2016.
- Shah, M. I., Mishra, S., Sarkar, M., and Rout, C. Identification of robust focus measure functions for the automated capturing of focused images from ZiehlNeelsen stained sputum smear microscopy slide. *Cytometry Part A*, 91(8):800–809, 2017. ISSN 15524930. doi: 10.1002/cyto.a.23142.
- Simonyan K., Z. A. Very deep convolutional networks for large-scale image recognition. *arXiv:1409.1556v6*, 2015.
- Skandarajah, A., Reber, C. D., Switz, N. A., and Fletcher, D. A. Quantitative imaging with a mobile phone microscope. *PLoS ONE*, 9(5), 2014. ISSN 19326203. doi: 10.1371/journal.pone.0096906.
- Skandarajah, A., Sunny, S. P., Gурpur, P., Reber, C. D., D’Ambrosio, M. V., Raghavan, N., James, B. L., Ramanjinappa, R. D., Suresh, A., Kandasarma, U., Birur, P., Kumar, V. V., Galmeanu, H. C., Itu, A. M., Modiga-Arsu, M., Rausch, S., Sramek, M., Kollegal, M., Paladini,

- G., Kuriakose, M., Ladic, L., Koch, F., and Fletcher, D. Mobile microscopy as a screening tool for oral cancer in India: A pilot study. *PLoS ONE*, 12(11):1–20, 2017. ISSN 19326203. doi: 10.1371/journal.pone.0188440.
- Smith, Z. J., Chu, K., Espenson, A. R., Rahimzadeh, M., Gryshuk, A., Molinaro, M., Dwyre, D. M., Lane, S., Matthews, D., and Wachsmann-Hogiu, S. Cell-phone-based platform for biomedical device development and education applications. *PLoS ONE*, 6(3), 2011. ISSN 19326203. doi: 10.1371/journal.pone.0017150.
- Tian J., C. L. Adaptive multi-focus image fusion using a waveletbased statistical sharpness measure. *IEEE Trans. Image Process*, 9:21372146, 2012.
- Wu, Y. C., Shiledar, A., Li, Y. C., Wong, J., Feng, S., Chen, X., Chen, C., Jin, K., Janamian, S., Yang, Z., Ballard, Z. S., Göröcs, Z., Feizi, A., and Ozcan, A. Air quality monitoring using mobile microscopy and machine learning. *Light: Science and Applications*, 6(9), 2017. ISSN 20477538. doi: 10.1038/lssa.2017.46. URL <http://dx.doi.org/10.1038/lssa.2017.46>.
- Xiangzhi Bai, Yu Zhang, F. Z. Quadtree-based multi-focus image fusion using a weighted focus-measure. *Elsevier*, 22:105–118, 2015.
- Xiaopeng Guo, Rencan Nie, J. C. FuseGAN: Learning to Fuse Multi-Focus Image via Conditional Generative Adversarial Network. *IEEE Trans. Image Process.*, 8: 2672–2680, 2019.
- Xiebo Genga, Sibio Liua, W. H. FFusionCGAN: An end-to-end fusion method for few-focus images using conditional GAN in cytopathological digital slides . *IEEE Trans. Image Process.*, 8:2672–2680, 2020.
- Y. Liu, S. Liu, W. Z. Multi-focus image fusion with dense sift. *IEEE Trans. Image Process.*, 23:139–155, 2015.
- Yang S., Berndl M., M. A. Assessing microscope image focus quality with deep learning. *BMC Bioinformatics*, 19(1), 2019. ISSN 21533539. doi: 10.1186/s12859-018-2087-4.
- Zhang Y., Liu Y., S. P. IFCNN: A general image fusion framework based on convolutional neural network. *IEEE Trans. Image Process.*, 9:99–118, 2020.